Synthesis, structure and magnetism of the new $S = 1$ kagome magnet $NH_4Ni_{2.5}V_2O_7(OH)_2.H_2O$

E T Connolly[1], P Reeves[1,2], D Boldrin[3] and A S Wills[1]

[1] Department of Chemistry, UCL, 20 Gordon St, London WC1H 0AJ
[2] Present address: Department of Material Science and Metallurgy, University of Cambridge, 27 Charles Babbage Road, Cambridge CB3 0FS, UK
[3] Department of Physics, Imperial College, Prince Consort Road, London SW7 2BZ, UK

E-mail: a.s.wills@ucl.ac.uk

Abstract. Kagome antiferromagnets (KAFMs) have long been known to host exotic electronic states due to their strong geometric frustration, including the quantum spin liquid (QSL) state in $S = \frac{1}{2}$ systems. Away from that limit, $S = 1$ KAFMs are also predicted to host unconventional ground states, such as spin nematic phases, but a paucity of studies on known model materials has restricted progress.

Here, we present the crystal structure and preliminary magnetization measurements on the newly synthesized $S = 1$ KAFM, $NH_4Ni_{2.5}V_2O_7(OH)_2.H_2O$, which has the 3-fold symmetry of the kagome lattice but significant site depletion, with ~ 77 % site occupancy. Bulk magnetic data show clear evidence of frustration and competition between ferromagnetic and antiferromagnetic interactions. We propose that the magnetic Hamiltonian is frustrated and that anisotropic terms cause the formation of an unconventional ground state.

Submitted to: *J. Phys.: Condens. Matter*

1. Introduction

Quantum frustrated magnets are a class of materials that display unconventional magnetic ground states and physical properties that arise when conventional Néel order is frustrated. Since the 1990s, many research efforts have focused on the search for quantum spin-liquids as they are predicted to host exotic properties, including quasiparticle excitations [1]. Much of this search has concentrated on 2-dimensional systems as the reduced dimensionality weakens the tendency for long-ranged order but still allows highly non-trivial states to form. Particular attention is paid to systems that feature the 2-dimensional kagome lattice of vertex sharing triangles as these can host macroscopically degenerate ground states that support the formation of dynamic superpositions of entangled spins [2]. The best known experimental examples of kagome QSLs are herbertsmithite [3], $\gamma - ZnCu_3(OH)_6Cl_2$, and kapellasite

[4, 5], $\alpha - ZnCu_3(OH)_6Cl_2$, $S = \frac{1}{2}$ kagome magnets based on the atacamite mineral family. These materials show that additional terms in the magnetic Hamiltonian beyond the simple nearest-neighbor Heisenberg model do not necessarily prevent the formation of QSL order. Rather, terms such as next-nearest neighbour, ferromagnetic, Dzyaloshinskii-Moriya (DM) exchange and spin anistropy are able to allow different 'flavours' of QSL to form, such as the largely nearest-neighbor QSL in herbertsmithite or the chiral-spin liquid in kapellasite. They can also lead to states where frozen and dynamic spins coexist, such as in $BaCu_3V_2O_8(OH)_2$ [6–8].

$S = 1$ magnets are between quantum and classical systems, as the role of quantum fluctuations is reduced in comparison to the $S = \frac{1}{2}$ systems, but the high frustration of the kagome lattice can still produce novel ground states. A notable example is the spin liquid hexagonal singlet state (HSS) predicted for a $S = 1$ kagome antiferromagnet (KAFM), where the integer spins are modeled as $S = \frac{1}{2}$ ferromagnetic-dimers [9–11]. In this state, each virtual $S = \frac{1}{2}$ spin in the ferromagnetic-dimer forms an entangled singlet around the hexagons of the kagome lattice. Possible example HSS magnets are the $S = 1$ KAFM materials m-MPYNN·BF_4 and NaV_6O_{11}, where NMR and single-crystal susceptibility data have shown these to display the gapped singlet ground state characteristic of HSS formation [12, 13]. Moving away from the kagome geometry itself, much of the research has also been done on the kagome staircase material $Ni_3V_2O_8$, following the discovery of multiferroic behavior caused by an incommensurate magnetic structure that simultaneously breaks time-reversal and space inversion symmetry [14,15].

As with their $S = \frac{1}{2}$ analogues, frustrated $S = 1$ magnets may have additional energy terms that add to the richness of magnetic phases. In these systems quadrupolar ordering *via* biquadratic exchange is possible and is predicted to produce nematic spin states. Such states consist of uniaxially aligned spins that break $O(3)$ rotational symmetry but retain time-reversal symmetry [16]. A $S = 1$ XXZ kagome model with large uniaxial spin-anisotropy and nearest-neighbor ferromagnetic exchange is predicted to host such a spin nematic state [17]. In the $S = 1$ isotropic KAFM $[C_6N_2H_8][NH_4]_2[Ni_3F_6(SO_4)_2]$, a net moment observed below 10 K matches expectations of an in-plane polarized state produced by moderate DM exchange [18, 19]. Other $S = 1$ kagome materials include: KV_3GeO_9 [20, 21], $(NH_4)(C_2H_8N)[V_2F_{12}]$ [22], $BaNi_3V_2O_8(OH)_2$ [23] and $YCa_3(VO)_3(BO_3)_4$ [24], which have undergone initial magnetic characterization but no analysis of their magnetic phases has been undertaken. While these materials show that $S = 1$ kagome-based magnets are capable of displaying exotic physics, there remain only a few well studied systems and additional studies are needed to map the phase space of possible ground states.

Here we introduce a new $S = 1$ kagome magnet $NH_4Ni_{2.5}V_2O_7(OH)_2.H_2O$ and present its synthesis, crystal structure and bulk magnetic properties. Despite significant depletion of the kagome sites, magnetic frustration is evidenced in the bulk magnetometry by a build-up of superparamagnetic domains at $T \leq 170$ K and suppression of the ordering transition to $T_C \sim 17$ K ($\theta_W = -42$ K). Analysis of the superexchange angles indicates that the frustration arises from a competition between

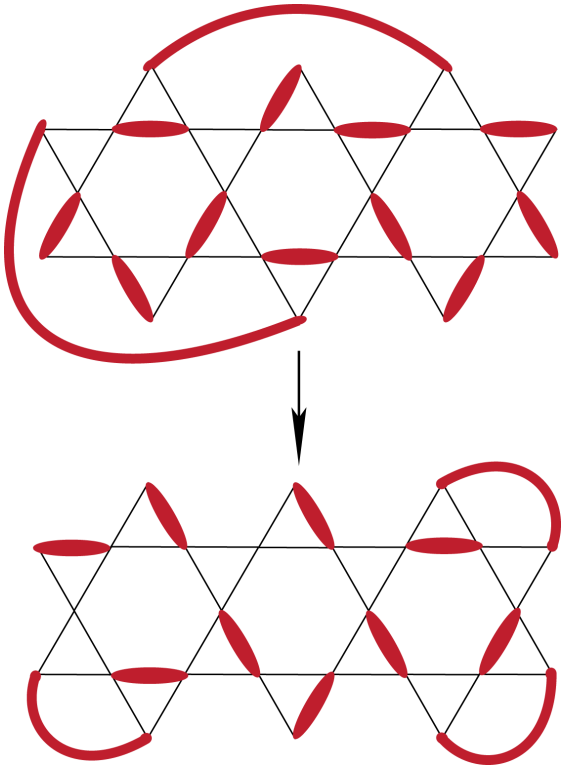

Figure 1. Schematic of a kagome structure hosting a QSL state. The short and long range entangled spins are highlighted in red (colour online). The entangled singlet states are randomly arranged over the kagome lattice. The degeneracy of the ground state allows for zero-point energy fluctuations to other disordered arrangements, indicated by the arrow.

nearest-neighbor ferromagnetic and antiferromagnetic exchange terms. Our results point to an unconventional ground state with contributions from additional energy terms, such as DM exchange and single-ion anisotropy.

2. Synthesis

The synthesis of $NH_4Ni_{2.5}V_2O_7(OH)_2.H_2O$ was adapted from that of $NH_4Zn_{2.5}V_2O_7(OH)_2.H_2O$ [25]. The synthesis here was scaled down (to 30 % of the literature quantities) and can be carried out within a given temperature window, as impurities were found to form at $T \leq 80\,^{\circ}$C and $T \geq 130\,^{\circ}$C. A phase pure sample was obtained as follows: NH_4OH (0.62 ml, 32 % wt, Sigma-Aldrich) was diluted with distilled water (3.88 ml). To this solution, V_2O_5 (166 mg, 99.6 %, Aldrich) was added and the suspension was stirred for 1 hour, whereupon it turned yellow. $NiSO_4.6H_2O$ (311 mg, $\geq$ 99.0 %, Aldrich) dissolved in distilled water (3.0 ml), was added to the yellow suspension and the reaction was left stirring for 1 hour to homogenize. This produced a turquoise gel which was loaded into a Pyrex pressure tube (15 ml, Ace Glass Inc.) and suspended in a silicon oil bath at 115 °C for 24 hours. The product was washed 3 times with water *via* centrifugation and dried at 60 °C for 5 hours. A yellow powder of $NH_4Ni_{2.5}V_2O_7(OH)_2.H_2O$ was produced

in a yield of $\sim 46\,\%$.

The ratios of the final reagent used are 1 V_2O_5 : 2.2 $NiSO_4.6H_2O$: 11.5 NH_4OH : 236 H_2O. Powder XRD indicated that the product of the first reaction is NH_4VO_3. The pH of the second reaction was 9.6 both before and after the synthesis. We propose the following idealized reaction mechanism for the formation of $NH_4Ni_{2.5}V_2O_7(OH)_2.H_2O$:

$$V_2O_{5(s)} + 2NH_4OH_{(aq)} \rightarrow 2NH_4VO_{3(s)} + H_2O_{(l)}$$
$$2NH_4VO_{3(s)} + \frac{5}{2}NiSO_4.6H_2O_{(aq)} + 4NH_4OH_{(aq)} \rightarrow NH_4Ni_{2.5}V_2O_7(OH)_2.H_2O_{(s)}$$
$$+\frac{5}{2}(NH_4)_2SO_{4(aq)} + 15H_2O_{(l)}$$

The reagent ratios for 1 M of $NH_4Ni_{2.5}V_2O_7(OH)_2.H_2O$ according to the idealized reaction scheme are 1 V_2O_5 : 2.5 $NiSO_4.6H_2O$: 6 NH_4OH, indicating that our synthetic conditions correspond to a slight deficit of $NiSO_4.6H_2O$ and an excess of NH_4OH. The outlined synthetic procedure can be used to understand how variation of concentrations or reagents will affect the product.

3. Crystal structure determination

The powder XRD data were recorded on a STOE Stadi-P diffractometer using Cu-Kα_1 radiation ($\lambda = 1.5406\,$Å) with a rotating capillary sample holder ($d = 0.3\,$mm). As no crystal structure is known for $NH_4Ni_{2.5}V_2O_7(OH)_2.H_2O$, the starting lattice parameters, space group and atomic positions for the crystal structure model were based on the engelhauptite ($KCu_3V_2O_7(OH)_2Cl$) structure in the $P6_3/mmc$ space group [26]. Rietveld refinement was carried out using the TOPAS software package [27]. The data, final calculated fit and difference plots are shown in Fig. 2. Crystal structure information obtained from the refinement is displayed in Table 1; details of the data collection procedure and refinement are given in the supplementary information. All crystal structure figures were produced using VESTA [28].

3.1. Structural characterization

Atomic positions were assigned to sites equivalent to those in the similarly structured engelhauptite [26]. NH_4^+ and H_2O units of $NH_4Ni_{2.5}V_2O_7(OH)_2.H_2O$ were found to reside in the respective framework cavities of Cl^- and K^+ in engelhauptite. NH_4^+ was placed in the Cl^- site despite the opposing charge. With respect to engelhauptite, we raise the possibility that difficulties in distinguishing Cl^- and K^+ could have led to misassignment of their positions. Our positioning of NH_4^+ and H_2O units maximizes hydrogen bonding, and improved the refinement so that the N site thermal parameter reached a physically meaningful value. It also matches the cavity assignment of K^+ and H_2O in $KZn_2.5V_2O_7(OH)_2.H_2O$, a vanadate with a comparable structure to $NH_4Ni_{2.5}V_2O_7(OH)_2.H_2O$ [29]. Structural refinements indicated that the O(w) site

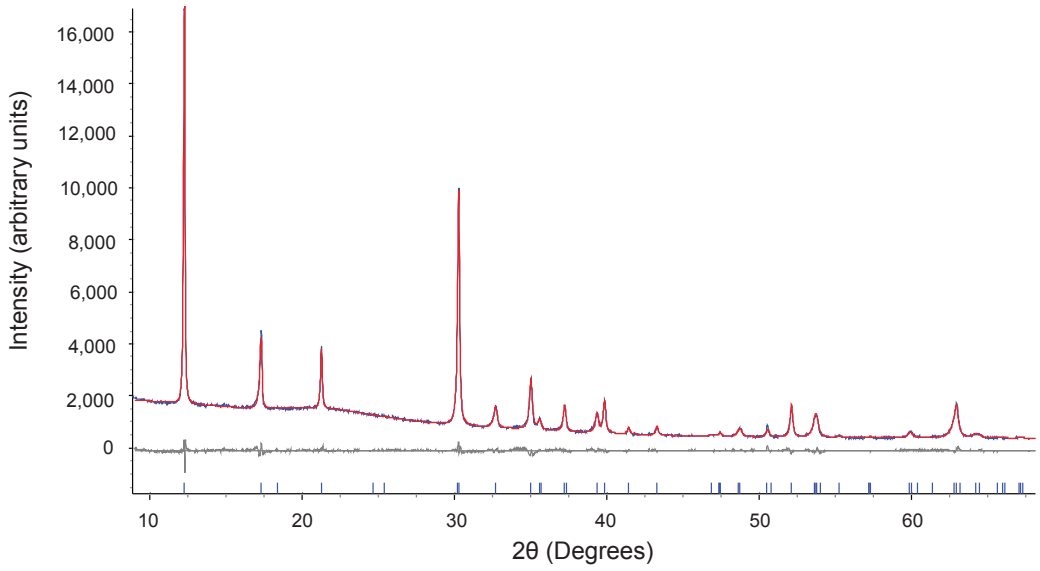

Figure 2. Rietveld refinement of XRD data measured on a powdered sample of $NH_4Ni_2.5V_2O_7(OH)_2.H_2O$ at a wavelength of $\lambda = 1.5406$ Å. The red, blue and grey lines, and blue markers represent the fit, data, difference plot and reflection positions, respectively. The final goodness-of-fit parameter was $\chi^2 = 2.35$ with 56 variables.

Name	Wyckoff site	x	y	z	B_{iso} (Å^2)	Occ.
Ni	$6g$	$\frac{1}{2}$	$\frac{1}{2}$	0	1.83(10)	0.7742(69)
V	$4e$	0	0	0.37362(16)	1.36(12)	1
O(1)	$12k$	0.15652(72)	0.3130(14)	0.59008(28)	2.40(20)	1
O(2)	$2b$	0	0	$\frac{1}{4}$	3.55(27)	1
O(H)	$4f$	$\frac{1}{3}$	$\frac{2}{3}$	0.06346(53)	1.83(26)	1
O(w)	$6h$	0.3800(44)	0.7601(87)	$\frac{3}{4}$	1.3(20)	0.217(11)
N	$2d$	$\frac{1}{3}$	$\frac{2}{3}$	$\frac{3}{4}$	1.87(98)	0.936(30)
H(1)	$4f$	$\frac{1}{3}$	$\frac{2}{3}$	0.135	5.7 [31]	1
H(2)	$24l$	0.64126	0.44028	0.76082	5.7 [31]	$= \frac{Ow_{occ}}{2}$
H(3)	$24l$	0.24415	0.76024	0.73145	5.7 [31]	$= \frac{N_{occ}}{4}$
H(4)	$4f$	$\frac{1}{3}$	$\frac{2}{3}$	0.81132	5.7 [31]	$= \frac{N_{occ}}{2}$

Table 1: Crystallographic information for $NH_4Ni_2.5V_2O_7(OH)_2.H_2O$ ($P6_3/mmc$, $a = 5.9159(2)$ Å, $c = 14.4430(6)$ Å). H_2O and NH_4^+ rigid bodies fix the respective hydrogen positions and occupancies relative to O(w) and N, H thermal parameters are from the literature.

features significant disorder which was modeled as reduced occupation of the $6h$ site. To help reveal how hydrogen bonding could stabilize the positions of these species, rigid bodies were defined with the bond lengths and angles set as the following for NH_4^+: N–H(3,4) = 0.974 Å, ∠H(3,4)–N–H(3,4) = 109.5° [30]; and for H_2O: O(w)–H(2) = 1.019 Å,

Interatomic distances (Å)		Angles (°)	
Ni-O(H)	1.9382(38)	Ni-O(H)-Ni	99.47(25)
Ni-O(1)	2.1903(38)	Ni-O(1)-Ni	84.94(19)
		O(1)-Ni-O(1)	91.51(34)
		O(H)-Ni-O(1)	92.39(17)
V-O(2)	1.7855(23)	V-O(2)-V	180.00
V-O(1)	1.6874(72)	O(2)-V-O(1)	108.11(17)
N-H(4)···O(1)	2.3045(62)		
N-H(3)···O(1)	2.2217(45)		
O(H)-H(1)···O(w)	1.728(14)		

Table 2: Selected bond distances and angles from the refined structure of $NH_4Ni_{2.5}V_2O_7(OH)_2.H_2O$

O(H)–H(1) = 1.008 Å; and the OH^- group: ∠H(3)–O(w)–H(3) = 109.5° [31]

During the refinement, the site occupancy of the divanadate and hydroxide groups were fixed to be unity while the occupancies of the Ni^{2+}, NH_4^+ and H_2O groups were freely refined. The occupancy of the Ni on the 6*g* site was freely refined to a value of ∼ 77%, which is close to the idealized stoichiometric value of 83 %. Our refined structural formula is $NH_4Ni_{2.31}V_2O_7(OH)_2.H_2O$.

3.2. Structural analysis

Selected bond distances and angles which are pertinent to the magnetic properties of $NH_4Ni_{2.5}V_2O_7(OH)_2.H_2O$ are displayed in Table 2 and the refined crystal structure is displayed in Fig. 3. The magnetic moments reside on brucite-type Ni-octahedra sheets that are separated by pyrovanadate pillars and interstitial pores, the latter contain NH_4^+ and H_2O. The interlayer Ni–Ni separation of 7.22 Å is very similar to that of volborthite [31] (7.21 Å), suggesting that the superexchange between layers will be very weak and the magnetic Hamiltonian is highly 2-dimensional. The local geometry of the V_2O_7 pillars differs between the two materials – in volborthite they are staggered while those of $NH_4Ni_{2.5}V_2O_7(OH)_2.H_2O$ are eclipsed.

The moment-bearing Ni^{2+} ions occupy the 6*g* site and have point symmetry $2/m$. They form an isotropic kagome lattice that is made up of identical equilateral triangular units of side 2.958 Å. The isotropic kagome lattice has a ground state Hamiltonian with few exchange terms and so the material is expected to follow the simple models of theory. The significant depletion of the kagome lattice through site vacancies is expected to lessen the magnetic frustration [32], QSL physics may still occur as the occupancy is still higher than the site percolation threshold for a kagome (p_c^{site}=65%) [33]. Entanglement of spins at greater separation than nearest neighbor could occur, which may further stabilize exotic quantum states. We note that similar levels of site disorder are seen in some kapellasite samples where they do not destroy its QSL ground state [4].

The Ni–Ni nearest-neighbor superexchange interactions in $NH_4Ni_{2.5}V_2O_7(OH)_2.H_2O$

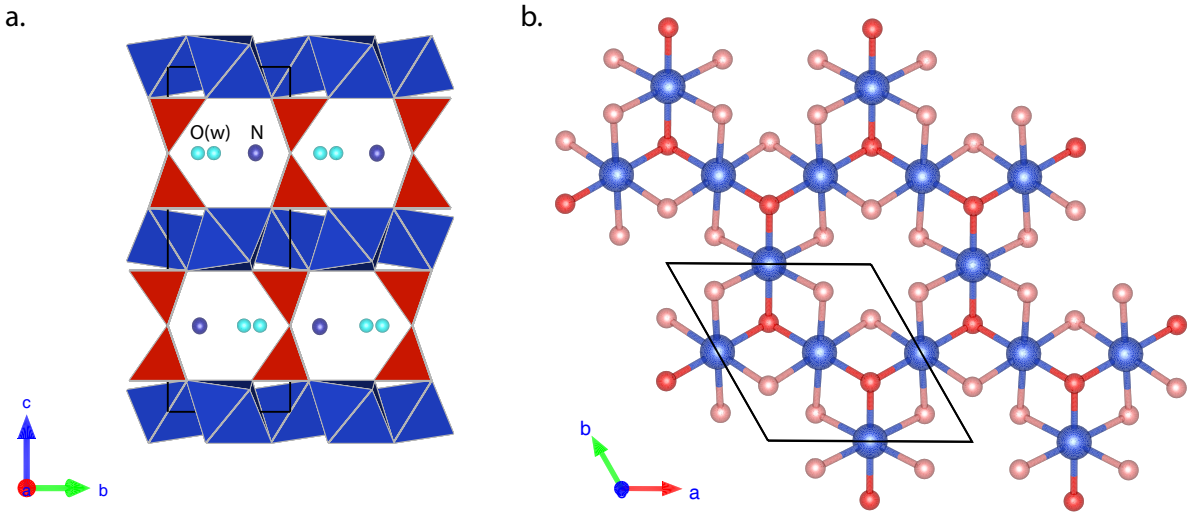

Figure 3. **a.** The structure of $NH_4Ni_2.5V_2O_7(OH)_2.H_2O$ observed down the a-axis. The Ni-octahedra sheets and bivanadate layers are illustrated in blue and red, respectively. The oxygen of the H_2O and the Nitrogen of the NH_4^+ are shown in the interstitial sites. **b.** The kagome plane viewed down the c-axis. The Ni^{2+} ions (blue) sit on a $6g$ site of the $P6_3/mmc$ space group which has 3-fold rotational symmetry. The Ni^{2+} ions ferromagnetic and antiferromagnetic superexchange pathways *via* the O(1) (pink) and O(H) (red) species, respectively, are shown.

are mediated by a bridging μ_3-OH group which sits on a $4f$ Wyckoff site with a 3-fold axis and a mirror plane. The bivanadate O(1) occupies a $12k$ Wyckoff site and lies on a mirror plane. The bridging angles of $\angle$ Ni–O(H)–Ni = 99.47(25)° and $\angle$ Ni–O(1)–Ni = 84.94(19)° are expected to mediate antiferromagnetic and ferromagnetic exchange, respectively, based on the Goodenough-Kanamori-Anderson rules [34,35]. Both interactions are predicted to be weak as the angles of these pathways are close to the cross-over angle of 90° where both ferromagnetic and antiferromagnetic exchange are minimal [36], their competition may reduce the overall strength of nearest-neighbor exchange.

Looking more closely at the environment of the Ni, we find its coordination octahedra have an unusual tetragonal distortion with axially compressed Ni–OH=1.9382(38) Å and equatorially elongated Ni–O(1)=2.1903(38) Å bonds. This distortion is likely to be the result of the structural requirements of the rigid bivanadate pillars which restrict the spacing between kagome planes to be approximately 7.22 Å. In order to allow the H_2O to occupy the interstitial site the O–H unit needs to move out of the interstitial cavity causing a compression of the Ni–O(H) bond. Similar Ni-octahedral distortions are observed in the kagome magnets $NH_4HNi_2Mo_2O_8(OH)_2$ and $BaNi_3V_2O_8(OH)_2$, where the restrictions of the rigid MO_4 and VO_4 tetrahedra force the unusual geometry [23, 37].

Our refinements also show displacement of the H_2O from the $2c$ site. This allows the hydrogens to point below the ab-plane of the O(w) site, as is observed in

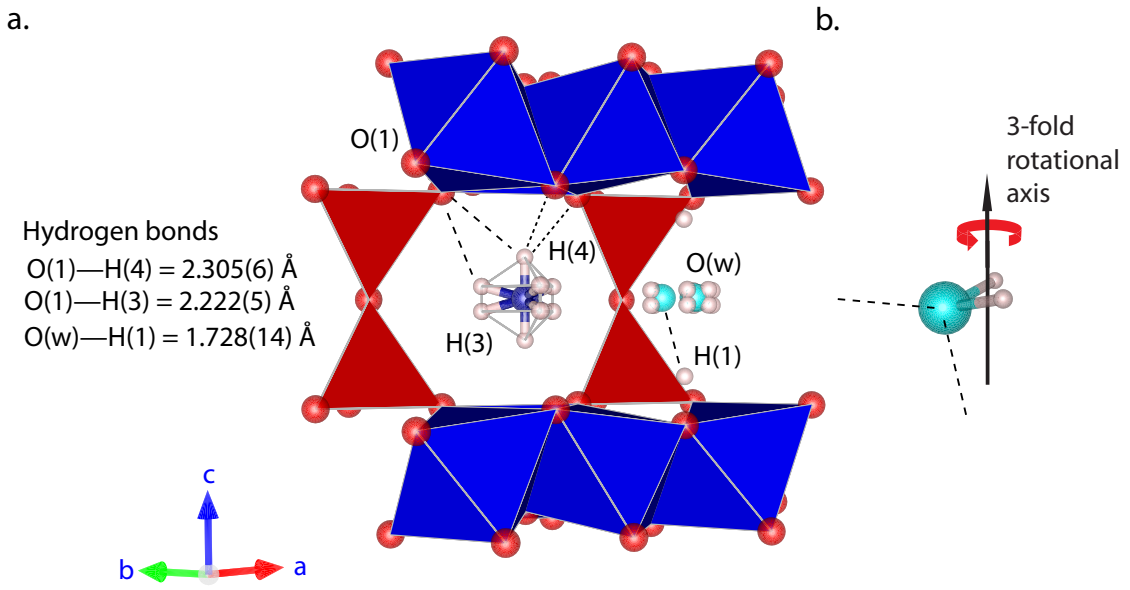

Figure 4. **a** The interstitial NH_4^+ and H_2O molecules are displayed sitting on the disordered sites between the Ni-octahedra sheets that make up the kagome layers. NH_4^+ has two equivalent energy orientations that are mirror images in the *ab*-plane. N-H(4) lies along the *c*-axis and forms three equivalent hydrogen bonds with O(1). The N–H(3) bonds lie on the planes of the 3-fold axis and H(3) forms hydrogen bonds with the O(1) of the vanadate units. O(w) lies off the 3-fold axis and hydrogen bonds to H(1). **b** A single H_2O rigid body is displayed with the hydrogens canted out of the *ab*-plane as observed in volborthite [38]: the lone pairs of O(w) are pointing at H(1) for hydrogen bonding.

volborthite [38]. This geometry would allow the lone pair orbitals of O(w) to point towards H(1), forming O(H)–H(1)$\cdots$O(w) = 1.728 Å (Fig. 4). The NH_4^+ unit would maximize hydrogen bonding with the V_2O_7 unit through 3 equivalent N–H(4)$\cdots$O(1) = 2.305 Å and N–H(3)$\cdots$O(1) = 2.222 Å hydrogen bonds, this orientation is expected to stabilize the eclipsed form of the V_2O_7 unit over the staggered phase observed in volborthite [38]. Determining the orientations of these extra-framework molecules is necessarily speculative from our X-ray diffraction data and we encourage studies using neutron diffraction on a deuterated sample.

4. Magnetic characterisation

Zero-field cooled and field-cooled magnetisation data were collected from $NH_4Ni_{2.5}V_2O_7(OH)_2.H_2O$ (131.8 mg) using the vibrating sample magnetometer of a Quantum Design PPMS-9T in a field of 1000 Oe and with heating rate of 2 K/min. Inspection of $\frac{1}{\chi}$ *vs.* T shows a linear Curie-Weiss regime over the range $170 \leq T \leq 300$ K from which a Weiss temperature of $\theta_W \simeq -42$ K can be extrapolated. The deviation from linear behavior on cooling below 170 K indicates that while spin correlations are building up, ordering is suppressed to a temperature below $T = |\theta_W|$: a well known characteristic of frustrated

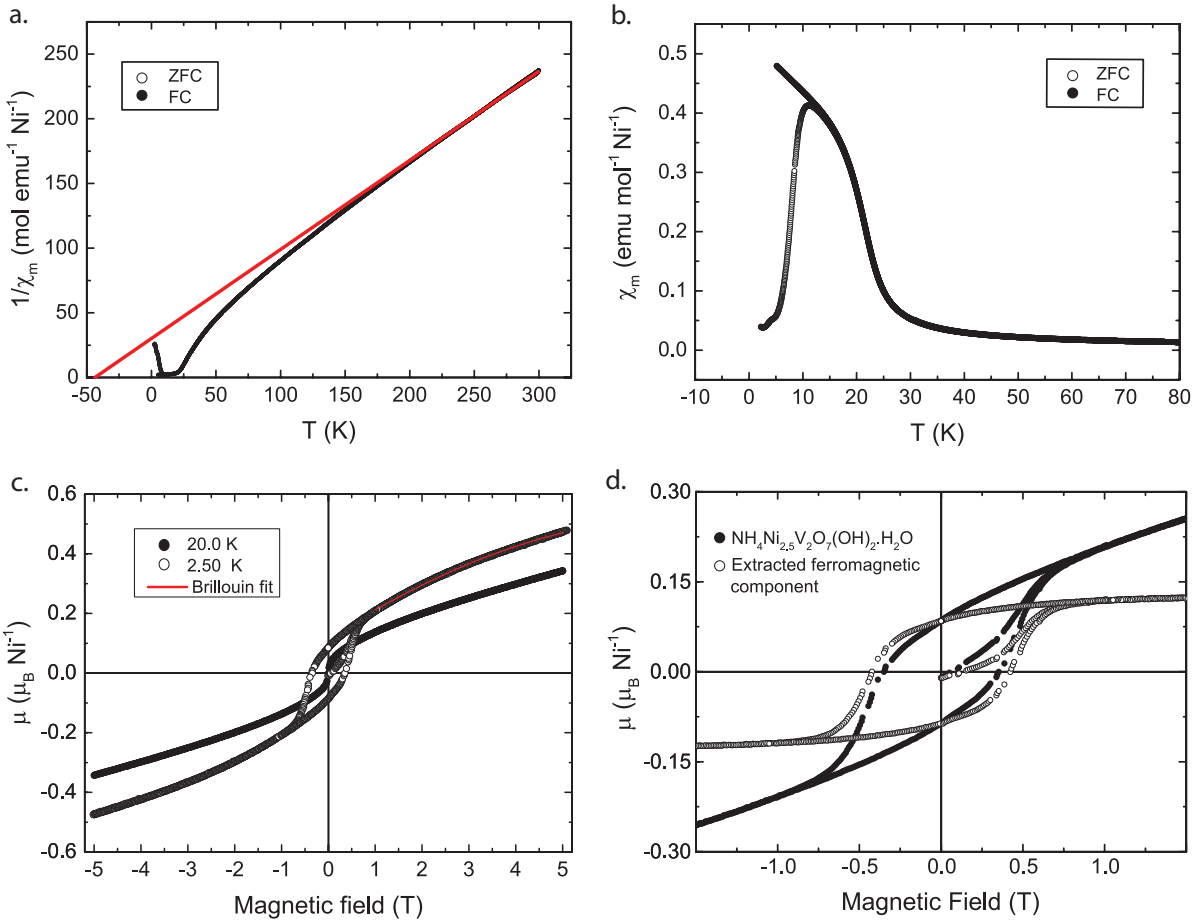

Figure 5. Bulk magnetization data collected for a sample of $NH_4Ni_{2.5}V_2O_7(OH)_2.H_2O$ **a.** The χ_m^{-1} *vs* T plot shows deviation from the linear Curie-Weiss law at $T \leq 170\,\mathrm{K}$ due to a build up of local spin correlations. Extrapolation from the linear region yields a of $\theta_W \simeq -42\,\mathrm{K}$ indicating an antiferromagnetic mean field. **b.** A plot of χ_m *vs* T shows a ferromagnetic component orders $\sim 17\,\mathrm{K}$ **c.** M *vs.* H at $2.5\,\mathrm{K}$ and $20\,\mathrm{K}$ confirm ferromagnetic ordering, the red line indicates the fit to the data with the adapted Brillouin function described in the text **d.** The collected data at $2.5\,\mathrm{K}$ (•) compared to the extracted ferromagnetic response (○)

magnets [5, 39, 40]. In contrast to the negative Weiss temperature, the temperature-dependance of the susceptibility indicates that there is a ferromagnetic-like transition at $T_C \sim 17\,\mathrm{K}$ that leads to a broad maximum. The juxtaposition of a ferromagnetic-like transition and a negative Weiss temperature agrees with the competing exchange interactions expected from our crystal structure analysis. The dominant character of the mean field, which would include contributions from further-neighbor exchange, appears to be antiferromagnetic and the transition only occurs when a ferromagnetic energy scale becomes dominant. From the room temperature value of the effective moment, $\mu_{\mathrm{eff}} = 3.18\ \mu_B$, a spin-only Landé g-factor of 2.25 can be calculated, in agreement with

the higher estimates for Ni^{2+} found in the literature [41].

The $M(H)$ data collected between -5 T and 5 T at 2.5 and 20 K (Fig. 5c) reveal a ferromagnetic component with field-dependent hysteresis. The field-dependence of the magnetization does not show saturation up to 5 T, confirming the coexistence of paramagnetism and ferromagnetism. This type of response is common in kagome magnets and is displayed in $S = \frac{1}{2}$ systems such as vesignieite, haydeeite, and Mg-herbertsmithite [40, 42, 43], and the $S = 1$ system $[C_6N_2H_8][NH_4]_2[Ni_3F_6(SO_4)_2]$ [19]. The contribution of the ferromagnetic and paramagnetic signals to similar hysteresis curves were previously isolated for the kagome magnet haydeeite using a paramagnetic Brillouin function and a factor that accounts for the ferromagnetic contribution to the saturated magnetization at low-field [44, 45]. Fits with such a Brillouin function to the magnetization of $NH_4Ni_{2.5}V_2O_7(OH)_2.H_2O$ at 2.5 K between 1 T and 5 T failed to accurately describe the field-dependence, as the build up of magnetic order means the assumption of non-interacting paramagnetic spins does not hold. The effect of interacting spins on the magnetization was previously modeled in Mn-doped CdTe [46] where the data is fitted with an adapted-Brillouin function that includes an effective temperature to account for interactions between the spins of the Mn^{2+} ions. In Mn-doped CdTe, and other systems fitted with this model [47, 48], reduced values of $M_{\rm sat}$ are observed, when compared to the theoretical ideal value. The increase in interactions between the spins means larger fields are required to saturate, as is observed for herbertsmithite at 0.4 K where the strong antiferromagnetic exchange prevents the magnetization from saturating in fields up to 50 T [49]. Based on these arguments, the following magnetization function was used to fit the $M(H)$ plots:

$$M(H)/M_{\rm sat} = (1 - f)B_{\rm J}(H) + f \tag{1}$$

Where $M_{\rm sat} = gJN\mu_{\rm B}$ and $B_{\rm J}$ is the adapted-paramagnetic Brillouin function per mole,

$$B_{\rm J}(H) = \frac{2J+1}{2J}\coth\left(\frac{2J+1}{2J}y\right) - \frac{1}{2J}\coth\frac{y}{2J} \tag{2}$$

Here, $y = g\mu_{\rm B}JH/k_{\rm B}T_{\rm eff}$ and $T_{\rm eff} = T + T_0$ where T_0 is a phenomenological parameter that accounts for antiferromagnetic interactions when positive [47]. Ni^{2+} is taken to be spin only, with $J = S = 1$ and $g = 2.25$, as calculated from the determined value of $\mu_{\rm eff}$. The values of T_0, f and $M_{\rm sat}$ are freely refined and the fit to data between 1 and 5 T at 2.5 K is displayed in Fig. 5c along with an extracted ferromagnetic component of $0.085\,\mu_{\rm B}\,{\rm Ni}^{-1}$. At 2.5 K, a value of $f = 0.203$ indicates that only a small fraction of spins contribute to the ferromagnetic signal. The refined value of $M_{\rm sat} = 0.604\,\mu_{\rm B}\,{\rm Ni}^{-1}$ is 27 % of the ideal theoretical value of $2.25\,\mu_{\rm B}\,{\rm Ni}^{-1}$ that indicates a slow rate of saturation with increasing field due to the build up of internal interactions. Similar reductions in $M_{\rm sat}$ are observed at $T < 2$ K for the KAFM materials herbertsmithite and barlowite of ~ 10 % and 48 % respectively [50, 51]. The $M_{\rm sat}$ reduction in barlowite has been related to a competition between ferromagnetic and antiferromagnetic exchange.

T (K)	T_0 (K)	f	$M_{\rm sat}$ ($\mu_{\rm B}$ Ni^{-1})
100	-	-	1.959(2)
50	-	-	1.957(10)
40	-30.42(6)	0.006(2)	0.475(2)
30	-23.19(7)	0.062(2)	0.461(3)
20	-12.18(9)	0.146(1)	0.545(4)
12.5	-5.30(7)	0.164(1)	0.584(4)
5	0.84(3)	0.174(1)	0.593(7)
2.5	2.82(3)	0.203(1)	0.604(2)

Table 3: The refined values for T_0, f and $M_{\rm sat}$ from the adapted Brillouin function given in Equations 1 and 2 for $M(H)$ plots collected at $T \leq 40$ K. $M_{\rm sat}$ values for 100 K and 50 K were refined using a standard Brillouin function [52]

Further magnetization against magnetic-field data were recorded between 1 T and 5 T at 5, 12.5, 30, 40, 50, and 100 K (Fig. 6a) in order to analyze the contributing interactions to the mean-field described by the adapted-Brillouin function. The data recorded at 100 K and 50 K were well fitted with a standard Brillouin function and required no additional parameters [52]. $M_{\rm sat}$ values of 1.959 $\mu_{\rm B}$ Ni^{-1} and 1.957 $\mu_{\rm B}$ Ni^{-1} were refined respectively, which are both close to the idealized value. Fits at temperatures $T \leq 40$ K required the adapted-Brillouin function. This change in behaviour follows the build up of magnetization that leads to a broad transition in $\chi(T)$ at $\sim$ 17 K (Fig. 5b). Values refined from the fits are given in Table 3 and plotted against temperature in Fig. 6b. f is found to be non-zero below $\sim$ 40 K and increases upon cooling, indicating that ferromagnetic behaviour is increasing, and is consistent with an increase in spontaneous moment at lower temperature (Fig. 5c). The value of $M_{\rm sat}$ drops sharply below $\sim$ 40 K due to the build up of interactions and then increases upon cooling as the ferromagnetic component strengthens. In contrast to the increased ferromagnetic contribution at low temperature, T_0 decreases upon cooling, indicating an increasing antiferromagnetic contribution and although this parameter is phenomenological it hints at complex ground state interactions.

Specific contributions to T_0 cannot be distinguished from this data. DM exchange has been found to cause ferromagnetic hysteresis in the $S = 1$ kagome staircase material $Ni_3V_2O_8$, by canting the spins away from the orientations preferred by the dominant nearest-neighbour antiferromagnetic exchange [14]. Structural similarities between $NH_4Ni_{2.5}V_2O_7(OH)_2.H_2O$ and the triangle-based $S = 1$ magnet $Li_2NiW_2O_8$ [53] however suggest that easy-axis spin-anisotropy plays a key role in the ground state of this new material.

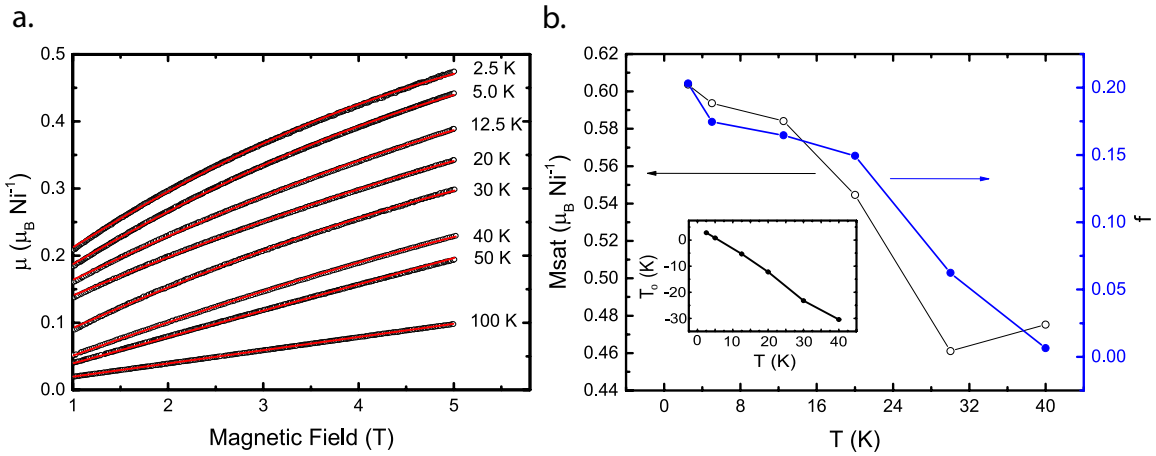

Figure 6. **a)** $M(H)$ data ($\circ$) collected at temperatures $\leq 100\,\mathrm{K}$ between 1 T to 5 T fit the adapted Brillouin function where three refinable parameters - M_{sat}, f, and T_0 - account for the interaction between spins **b)** The refined values of M_{sat} and f increase upon cooling. The change in f indicates the build up of a ferromagnetic response. This larger ferromagnetic response will increase the value of M_{sat} at low-field. **Inset:** The increase in T_0 with decreasing temperature indicates possible increase in antiferromagnetic interactions, in contrast to the observed increase in the ferromagnetic response

5. Conclusion

A hydrothermal synthesis and reaction mechanism for the production of pure crystalline samples of $NH_4Ni_{2.5}V_2O_7(OH)_2.H_2O$ has been outlined. The crystal structure of $NH_4Ni_{2.5}V_2O_7(OH)_2.H_2O$ consists of Ni^{2+} kagome-planes separated by $V_2O_7^{4-}$ pyrochlore pillars with ammonium and water groups residing in the interstitial sites; the orientation of the interstitial molecules have been speculated upon.

Preliminary magnetization measurements on $NH_4Ni_{2.5}V_2O_7(OH)_2.H_2O$ show that despite significant depletion of the magnetic site, it displays the suppression of magnetic ordering and superparamagnetic correlations that are characteristic of kagome antiferromagnets, and a ferromagnetic transition at $T_{\mathrm{C}} = 17\,\mathrm{K}$. The juxtaposition of these responses points to a complex ground state with an ordered component. The $\angle$Ni–O–Ni bond angles show competing nearest neighbor exchange which may produce a small value of J_{ij}. In such systems the low temperature Hamiltonian is often dominated by anisotropic energy terms such as DM exchange, easy-axis spin-anisotropy, or further neighbour exchange. Further to this, elastic and inelastic neutron scattering experiments would help determine the ground states of this material and how additional terms in the magnetic Hamiltonian affect $S = 1$ kagome systems.

6. Acknowledgments

We would like to thank Jeremy Cockcroft for informative discussions, Martin Vickers for experimental assistance, and University College London (UCL) for the provision of the studentship (1329860).

7. References

[1] Balents L 2010 *Nature* **464** 199
[2] Mendels P and Bert F 2016 *Comp. Ren. Phys.* **17** 455
[3] Han T H, Helton J S, Chu S, Nocera D G, Rodriguez-Rivera J A, Broholm C and Lee Y S 2012 *Nature* **492** 406
[4] Fåk B, Kermarrec E, Messio L, Bernu B, Lhuillier C, Bert F, Mendels P, Koteswararao B, Bouquet F, Ollivier J, Hillier A D, Amato A, Colman R H and Wills A S 2012 *Phys. Rev. Lett.* **109** 037208
[5] Colman R H, Ritter C and Wills A S 2008 *Chem. Mat.* **20** 2005
[6] Colman R H, Bert F, Boldrin D, Hillier A D, Manuel P, Mendels P and Wills A S 2011 *Phys. Rev. B* **83** 180416
[7] Quilliam J A, Bert F, Colman R H, Boldrin D, Wills A S and Mendels P 2011 *Phys. Rev. B* **84** 180401
[8] Zorko A, Bert F, Ozarowski A, van Tol J, Boldrin D, Wills A S and Mendels P 2013 *Phys. Rev. B* **88** 144419
[9] Hida K 2000 *J. Phys. Soc. Jpn.* **69** 4003
[10] Nishimoto S and Nakamura M 2015 *Phys. Rev. B* **14** 1
[11] Changlani H J and Läuchli A M 2015 *Phys. Rev. B* **91** 1
[12] Wada N, and Kobayashi T, Yano H, Okuno T, Yamaguchi A and Awaga K 1997 *J. Phys. Soc. Jpn.* **66** 4
[13] Kato H, Kato M, Yoshimura K and Kosuge K 2001 *J. Phys. Soc. Jpn.* **70** 1404
[14] Lawes G, Kenzelmann M, Rogado N, Kim K H, Jorge G A, Cava R J, Aharony A, Entin-Wohlman O, Harris A B, Yildirim T, Huang Q Z, Park S, Broholm C and Ramirez A P 2004 *Phys. Rev. Let.* **93** 14
[15] Lawes G, Harris A B, Kimura T, Rogado N, Cava R J, Aharony A, Entin-Wohlman O, Yildirim T, Kenzelmann M, Broholm C and Ramirez A P 2005 *Phys. Rev. Let.* **95** 1
[16] Andreev A F, and Grishchuk I A 1985 *Sov. Phys. JETP* **60** 297
[17] Damle K, and Senthil T 2006 *Phys. Rev. Let.* **97** 067202
[18] Behera J N and Rao C N R 2006 *J. Amer. Chem. Soc.* **128** 9334
[19] Behera J N and Rao C N R 2007 *Chem. Phys. Chem.* **8** 217
[20] Hara S, Sato H and Narumi Y 2012 *J. Phys. Soc. Jpn.* **81** 1
[21] Takagi E, Takuya A, Hara S, Sato H, Kimura T, Wakabayashi Y 2017 *Phys. Rev. B* **95** 060402
[22] Aidoudi F H, Downie L J, Morris R E, de Vries M A and Lightfoot P 2014 *Dalton. Trans.* **43** 6304
[23] Freedman D E, Chisnell R, McQueen T M, Lee Y S, Payen C and Nocera D G 2012 *Chem. Comm.* **48** 64
[24] Miiller W, Christensen M, Khan A, Sharma N, Macquart B, Avdeev M, Mcintyre G J, Piltz R O and Ling C D 2011 *Chem. Mater.* **3** 1315
[25] Hoyos D, Palacio L A, Paillaud J-L, Simon-Masseron A and Guth J-L 2004 *Solid State Sci.* **6** 1251 Ribeiro M F 2008 *J. Haz. Mat.* **153** 628
[26] Pekov I V, Siidra O I, Chukanov N V, Yapaskurt V O, Britvin S N, Krivovichev S V, Schüller W and Ternes B 2015 *Min. Petro.* **3** 1
[27] Bruxer AXS 2008 Topas v4: General profile and structure analysis software for powder diffraction data
[28] Momma K and Izumi F 2011 *J. Appl. Cryst.* **44** 1272
[29] Hoyos D, Paillaud J-L, Simon-Masseron A and Guth J-L 2005 *Solid State Sci.* **7** 616
[30] Hawthorne F C 1977 *J. Sol. St. Chem.* **170** 157
[31] Lafontaine M A, Le Bail A and Ferey G 1990 *J. Sol. St. Chem.* **85** 220
[32] Lacroix C, Mendels P and Mila F (eds) 2011 *Introduction to Frustrated Magnetism* (New York, USA: Springer)
[33] Feng X, Deng Y and Blöte H W J 2008 *Phys. Rev. E* **78** 1
[34] Goodenough J B 1955 *Phys. Rev.* **100** 564.

[35] Kanamori J 1959 *J. Phys. Chem. Sol.* **10** 87
[36] Nanda K K, Thompson L K, Bridson J N, Nag K, 1994 *J. Chem. Soc.* **8** 1337
[37] Levin D and Soled S L, Ying J Y 1996 *Inorg. Chem.* **35** 4191
[38] Hiroi Z, Hanawa M, Kobayashi N, Nohara M, Takagi H, Kato Y and Takigawa M 2001 *J. Phys. Soc. Jpn.* **70** 3377
[39] Hiroi Z, Yoshida H, Okamoto Y and Takigawa M 2009 *J. Phys. Conf. Ser.* **145** 012002
[40] Colman R, Sinclair A and Wills A S 2010 *Chem. Mat.* **22** 5774
[41] Iri T, Hirako S-I and Kambe K 1979 *J. Phys. Soc. Jpn.* **46** 106
[42] Colman R H, Sinclair A and Wills A S 2011 *Chem. Mat.* **23** 1811
[43] Yoshida H, Michiue Y, Takayama-Muromachi E and Isobe M 2012 *J. Mat. Chem.* **22** 18793
[44] Kermarrac E 2012 *Nouveaux états quantiques de spin induits par frustration magnétique sur le réseau kagome* Ph.D Thesis Université Paris Sud
[45] Boldrin D 2015 *Synthesis and Study of Quantum Kagome Magnets* Ph.D Thesis UCL
[46] Gaj J A, Planel R and Fishman G 1979 *Solid State Commun.* **29** 435
[47] Douglas K, Nakashima S and Scott J F 1984 *Phys. Rev. B* **29** 5602
[48] Douglas K, Shapira Y, Foner S, Khazai B, Kershaw R, Dwight K and Wold A 1984 *Phys. Rev. B* **29** 5634
[49] Han T -H, Chisnell R, Bonnoit C J, Freedman D E, Zapf V S, Harrison N, Nocera D G, Takano Y and Lee Y S arXiv:1402.2693
[50] Bert F, Nakamae S, Ladieu F, Hôte D L, Bonville P, Duc F, Trombe J, Mendels P 2007 *Phys. Rev. B* **76** 132411
[51] Han T -H, Singleton J and Schlueter J A 2014 *Phys. Rev. Lett.* **113** 227203
[52] Kittel C *Introduction to solid state physics*, 7th ed.; John Wiley & Sons, Inc.: New York, USA, 2004.
[53] Ranjith K M, Nath R, Majumder M, Kasinathan D, Skoulatos M, Keller L, Skourski Y, Baenitz M and Tsirlin A A 2016 *Phys. Rev. B* **94** 1
[54] Stephens P W 1999 *J. App. Crys.* **32** 281
[55] Roe R J and Krigbaum W R 1964 *J. Chem. Phys.* **40** 2608
[56] Young R A 2001 *The Rietveld Method* (New York, USA: Oxford University Press)

Appendix A. Supplementary information

Crystallographic data	
Chemical formula	$NH_4Ni_{2.5}V_2O_7(OH)_2.H_2O$
Crystal system	Hexagonal
Space group	$P6_3/mmc$ (194)
a (Å)	5.9159(2)
c (Å)	14.4436(6)
Volume (Å^3)	437.76(2)
Formula units (Z)	2
Data collection	
Radiation, λ (Å)	Cu Kα_1, 1.54
2θ-step size increments (°)	0.05
2θ range (°)	9 - 70
Geometry	Debye-Scherrer geometry
Temperature (K)	293
Zero error (°)	0.04777(5)
μR	1.6(4)
Number of observed reflections	53
Refinement	
Instrumental, unit cell and profile parameters	36
Peak area parameters	20
Profile function	Stephens' anisotropic broadening [54] Spherical harmonics [55]
R_{exp} [56]	1.43
R_{wp} [56]	3.34
χ^2 [56]	2.35

Table A1: Details of the data collection procedure and Rietveld refinement of $NH_4Ni_{2.5}V_2O_7(OH)_2.H_2O$ are displayed along with crystallographic data